System-level design for efficient execution of CNNs at the edge

Minakova, S.

Chapter 4

Methodology for low-memory CNN inference

Svetlana Minakova and Todor Stefanov. "Buffer Sizes Reduction for Memory-efficient CNN Inference on Mobile and Embedded Devices". *In Proceedings of 23rd Euromicro Conference on Digital System Design (DSD'20)*, pp. 133-140, Portoroz, Slovenia, August 26-28, 2020.

In this chapter, we present our methodology for low-memory CNN inference at the Edge, which corresponds to the second research contribution of this thesis summarized in Section 1.5.2. The proposed methodology is a part of the system-level optimization engine, introduced in Section 1.5, and is aimed at relaxation of Limitation 1, introduced in Section 1.4.1. The reminder of this chapter is organized as follows. Section 4.1 introduces, in more details, the problem addressed by our novel methodology. Section 4.2 gives a summary of the contributions, presented in the chapter. An overview of the related work is given in Section 4.3. Section 4.4 provides a motivational example. Section 4.5 presents the proposed methodology. Section 4.6 presents the experimental study performed by using the proposed methodology. Finally, Section 4.7 ends the chapter with conclusions.

4.1 Problem statement

As mentioned in Chapter 1 in Section 1.2, in order to be deployed and executed on an edge platform, a CNN is required to have low memory footprint. This is because modern edge platforms have limited memory resources. For example,

the basic version of the Raspberry Pi 4 [30] embedded platform has 1 GB of memory. For comparison, deployment and inference of the state-of-the-art VGG-19 CNN [4], requires about 700 MB of memory. If deployed on the Raspberry Pi 4, VGG-19 CNN would occupy almost all memory available on the platform and leave insufficient memory space for the operating system running on the platform, libraries required to execute the CNN inference, storage of the CNN input and output data, etc.

To enable inference of a state-of-the-art CNN such as VGG-19 on an edge platform such as Raspberry Pi 4, the CNN memory footprint should be reduced. To this aim, the CNN memory reduction methodologies [5,11,17,31, 73,76,98] have been proposed. The most common of these methodologies, namely pruning and quantization [11,17,31,98], reduce the memory footprint of a CNN by reducing the number or size of CNN parameters (weights and biases). However, at high memory reduction rates, these methodologies may decrease the CNN accuracy, while, as mentioned in Section 1.2, high accuracy is very important for most CNN-based applications. Moreover, for many state-of-the-art CNNs [4], the intermediate computational results, exchanged between CNN layers and stored in the platform memory during the CNN inference, take even more space than the CNN parameters. For example, for the MobileNet V2 [81] and DenseNet [40] CNNs, the intermediate computational results comprise up to 63% and 80% of the total CNN memory requirement, respectively[1]. For these CNNs, the memory reduction achieved only by methodologies such as pruning and quantization (i.e., only by reducing the amount of memory needed to store CNN parameters) may not be sufficient to fit the CNN into the memory of the target edge platform. In other words, CNN inference at the edge requires a methodology, which reduces the amount of memory required to store the intermediate computational results of a CNN, that is complimentary to the pruning and quantization methodologies. In this chapter, we propose such a methodology.

4.2 Contributions

We propose a novel methodology, which reduces the amount of memory required to store intermediate computational results of a CNN, thereby reducing the CNN memory footprint. Our proposed methodology is based on the ability of CNN operators to process data by parts, illustrated in Figure 2.2 and explained in Section 2.1. In our methodology, the execution of every CNN layer is performed in several *phases*, such that: 1) at each phase, the layer

[1]The percentage is given for the CNNs deployed and executed with no memory reduction

processes only a part of its input data; 2) phases are executed in a specific order; 3) the platform memory, allocated to store intermediate computational results of a CNN is reused between the data parts. As the data processing by parts may cause CNN execution time overheads (e.g. CNN layers may require time to switch among the data parts), our methodology may reduce the CNN throughput. However, unlike the most common pruning and quantization methodologies [11,17,31,98], our methodology does not change the number and precision of CNN parameters and therefore does not decrease the CNN accuracy. Thus, our methodology is orthogonal to the pruning and quantization methodologies, and can be combined with these methodologies for further CNN memory footprint reduction. Our proposed methodology, presented in Section 4.5, is our main novel contribution. Other important novel contributions are:

1. the phases derivation algorithm (see Section 4.5.1). This algorithm automatically derives the number of phases, performed by every CNN layer. The number of phases is computed such that at each phase, every layer of a CNN processes a minimum part of the layer input data and produces a minimum part of the layer output data. Thus, the phases derivation algorithm ensures that every layer requires minimum amount of memory to store its intermediate computational results at every phase;

2. the CNN-to-CSDF conversion algorithm (see Section 4.5.2). This algorithm automatically converts a CNN, represented as the CNN model (see Section 2.1) into a functionally equivalent CSDF model (see Section 2.5). Unlike the CNN model, the CSDF model has means for explicit specification of the CNN inference with phases. Thus, the CNN-to-CSDF conversion algorithm enables for CNN inference with phases, underlying our proposed methodology;

3. 2.8% to 38% CNN memory reduction, compared to the most relevant buffers reuse methodology, exploited by the well-known and widely used TensorRT [72] DL framework for CNN deployment and inference at the Edge (see Section 4.6).

Scope of work: in this chapter, we assume that every input CNN is executed with the smallest possible batch size (i.e., $batch = 1$) typical for CNN execution at the Edge. This restriction comes from the fact that data batching (i.e., using $batch > 1$) [35] is the opposite to the data processing by parts, used by our proposed methodology. The data processing by parts involves splitting of the intermediate CNN computational results into parts, which enables for

reduction of the CNN memory footprint at the cost of possible CNN throughput decrease. The data batching, on the other hand, involves aggregating the intermediate CNN computational results in the platform memory, which leads to increase of the CNN throughput at the cost of CNN memory footprint increase.

4.3 Related Work

The most common CNN memory reduction methodologies, namely pruning and quantization, reviewed in surveys [11,17,31,98], reduce the memory cost of a CNN by reducing the number or size of CNN parameters (weights and biases) [4]. However, at high memory reduction rates these methodologies decrease the CNN accuracy, whereas high accuracy is very important for many CNN-based applications [4]. In contrast, our memory reduction methodology does not change the CNN model parameters and therefore does not decrease the CNN accuracy. Moreover, our methodology reduces the platform memory occupied by the CNN intermediate computational results, while the pruning and quantization methodologies reduce the platform memory occupied by the CNN parameters (weights and biases). Therefore our methodology is orthogonal to the pruning and quantization methodologies, and can be combined with these methodologies for further CNN memory footprint reduction.

The Knowledge Distillation (KD) methodologies try to shift knowledge from an initial CNN into another CNN, with smaller size but with the same accuracy. However, KD methodologies involve training from scratch and do not guarantee that the accuracy of the initial CNN can be preserved. Moreover, KD methodologies can only be applied to CNNs designed to perform classification [17], while many CNNs are designed to perform other tasks, such as object detection or segmentation [4]. In contrast, our memory reduction methodology is a general systematic methodology, which always guarantees preservation of the CNN accuracy, and is not limited to CNNs designed to perform classification tasks.

The CNN layers fusion methodologies, such as the methodologies [5,73] and the methodologies adopted by DL frameworks, such as TensorRT [72] or PyTorch [75], enable to reduce the CNN memory cost by transforming the network into a simpler form but preserving the same overall behavior. Being a part of the CNN model definition, the CNN layer fusion methodologies are orthogonal to our proposed methodology and can be combined with our methodology for further CNN memory optimizations. In our experimental study (Section 4.6), we implicitly use the CNN layers fusion by implementing

the CNNs inference with the TensorRT DL framework [72], which has built-in CNN layers fusion.

The buffers reuse methodologies, such as the methodology proposed in [76] and the methodology, employed by the TensorRT framework for efficient CNN inference at the edge [72], reduce the CNN memory footprint by sharing memory between CNN layers, executed at different computational steps. However, these methodologies do not reuse memory within CNN layers. As a result, these methodologies are not very efficient for: 1) CNNs with residual connections, such as ResNets [36] and DenseNets [40], because in these CNNs the data associated with different layers has to be stored for many computational steps; 2) CNNs that process high-resolution input data, because in these CNNs one layer can occupy significant amount of platform memory to store its input and output data. In contrast, our methodology reuses memory within layers of a CNN, which makes our methodology more efficient at reducing the memory of CNNs that have residual connections or/and process high-resolution data. We note that the CNN buffers reuse methodologies are the only methodologies among the related work that can be directly compared to other proposed methodology. Other related works, discussed above, are either orthogonal to our proposed methodology (e.g., pruning and quantization methodologies [11,17,31,98]) or cannot be directly compared to our proposed methodology (e.g., the KD methodologies [17]). Therefore, in our experimental results (see Section 4.6), we compare our methodology only to the buffers reuse methodologies. More precisely, we compare our methodology to the buffers reuse methodology, exploited by the TensorRT [72] DL framework.

4.4 Motivational Example

Layers of a CNN do not process their input data at once. As shown in Figure 2.2 and explained in Section 2.1, to process its input data, a layer of a CNN moves along the input data with a sliding window, applying an operator to the parts of the input data. In this section, we show how this feature can be used to reduce the memory cost of a CNN. We define the processing of an input data part by a layer as a *phase*. If a layer has one phase, it processes its input data as one part. If a layer has two phases, it processes its input data in two parts, etc.

In Table 4.1, we give four examples (Ex1, Ex2, Ex3, Ex4) of inference of the CNN, shown in Figure 4.1 and represented as the CNN model, introduced in Section 2.1. In each of these examples the CNN inference is executed on the Jetson TX2 platform introduced in Section 2.3 and shown in Figure 2.4. Every layer of the CNN is executed in one or multiple phases. For every

Table 4.1: *Execution of CNN inference with phases*

Ex.	Layer phases					Phases execution order	Buffer sizes (Bytes)					Thr. (fps)
	l_1	l_2	l_3	l_4	l_5		B_1	B_2	B_4	B_5	Total	
Ex1	$X_{1k} = \emptyset$, $Y_{1k}^{[1,32,32,1]}$ Φ_1=1	$X_{2k}^{[1,32,32,1]}$, $Y_{2k}^{[1,16,16,4]}$ Φ_2=1	$X_{3k}^{[1,16,16,4]}$, $Y_{3k}^{[1,4,4,3]}$ Φ_3=1	$X_{4k}^{[1,4,4,3]}$, $Y_{4k}^{[1,1,1,2]}$ Φ_4=1	$X_{5k}^{[1,1,1,2]}$, $Y_{5k} = \emptyset$ Φ_5=1	$l_{11}, l_{21}, l_{31}, l_{41}, l_{51}$	1024	1024	48	2	2098	334
Ex2	$X_{1k} = \emptyset$, $Y_{1k}^{[1,24,32,1]}$ Φ_1=2	$X_{2k}^{[1,24,32,1]}$, $Y_{2k}^{[1,8,16,4]}$ Φ_2=2	$X_{3k}^{[1,16,16,4]}$, $Y_{3k}^{[1,4,4,3]}$ Φ_3=1	$X_{4k}^{[1,4,4,3]}$, $Y_{4k}^{[1,1,1,2]}$ Φ_4=1	$X_{5k}^{[1,1,1,2]}$, $Y_{5k} = \emptyset$ Φ_5=1	$l_{11}, l_{21}, l_{12}, l_{22}, l_{31}, l_{41}, l_{51}$	768	1024	48	2	1842	333
Ex3	$X_{1k} = \emptyset$, $Y_{1k}^{[1,1,32,1]}$ Φ_1=32	$X_{2k}^{[1,17,32,1]}$, $Y_{2k}^{[1,1,16,4]}$ Φ_2=16	$X_{3k}^{[1,16,16,4]}$, $Y_{3k}^{[1,4,4,3]}$ Φ_3=1	$X_{4k}^{[1,4,4,3]}$, $Y_{4k}^{[1,1,1,2]}$ Φ_4=1	$X_{5k}^{[1,1,1,2]}$, $Y_{5k} = \emptyset$ Φ_5=1	$l_{1(1-17)}, l_{21}, [l_{1(18-32)}, l_{2(2-16)}], l_{31}, l_{41}, l_{51}$	544	1024	48	2	1618	310
Ex4	$X_{1k} = \emptyset$, $Y_{1k}^{[1,1,32,1]}$ Φ_1=32	$X_{2k}^{[1,17,32,1]}$, $Y_{2k}^{[1,1,16,4]}$ Φ_2=16	$X_{31}^{[1,6,16,4]}$, $X_{32}^{[1,5,16,4]}$, $X_{33}^{[1,5,16,4]}$, $X_{34}^{[1,6,16,4]}$, $Y_{3k}^{[1,1,4,3]}$ Φ_3=4	$X_{4k}^{[1,4,4,3]}$, $Y_{4k}^{[1,1,1,2]}$ Φ_4=1	$X_{5k}^{[1,1,1,2]}$, $Y_{5k} = \emptyset$ Φ_5=1	$l_{1(1-17)}, l_{21}, [l_{1(18-22)}, l_{2(2-6)}], l_{31}, [l_{1(23-25)}, l_{2(7-9)}], l_{32}, [l_{1(26-28)}, l_{2(10-12)}], l_{33}, [l_{1(29-32)}, l_{2(13-16)}], l_{34}, l_{41}, l_{51}$	544	384	48	2	978	308

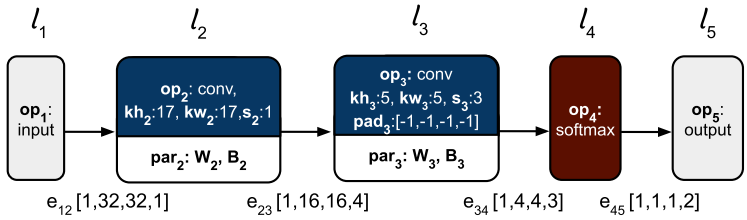

Figure 4.1: *Example CNN*

layer $l_i, i \in [1,5]$, Columns 2 to 6 in Table 4.1 list: 1) the number of phases Φ_i; 2) part X_{ik} of the input data X_i, processed by layer l_i at its k-th phase, $k \in [1,\Phi_i]$; 3) part Y_{ik} of the output data Y_i, produced by layer l_i at its k-th phase, $k \in [1,\Phi_i]$. The data parts are annotated with the shape, introduced for CNN data tensors in Section 2.1. Recall that in this thesis, every data tensor is represented as a 4-dimensional tensor of shape $[batch, h, w, ch]$, where $batch, h, w, ch$ are the tensor batch size, the height, the width, and the number of channels, respectively. All phases are executed in a specific order, given in Column 7, where l_{ik} denotes the execution of the k-th phase of layer l_i. The execution order ensures functional equivalence of all examples, given in Table 4.1, and allows to reduce the CNN buffer sizes as explained below. Columns 8 to 12 in Table 4.1 show the sizes of the CNN buffers, introduced in Section 2.2, i.e., segments of platform memory, allocated to store intermediate computational results, produced by the CNN layers. Every CNN edge e_{ij} is allocated its own buffer B_k. The size of each buffer is computed using Equation 2.8 explained in Section 2.2 with the assumption that one element in any CNN data tensor requires 1 byte of memory for its storage. Column 13 in Table 4.1 shows the CNN throughput in frames per second (fps). As shown in Column 13, the CNN inference throughput differs for examples Ex1, Ex2, Ex3, Ex4. This is because data processing by parts may cause CNN execution time overheads (e.g. CNN layers may require time to switch among the data parts), leading to CNN throughput decrease. The more phases are performed by a CNN (i.e., the more data parts are accepted and produced by the CNN layers), the larger the throughput overhead is. For example, the throughput of Ex4, where the CNN layers processes data in 32, 16, 4, 1 and 1 phases respectively, is 26 fps smaller than the throughput of Ex1, where every CNN layer processes data in one phase.

Example Ex1, given in Row 3 of Table 4.1, describes the CNN inference typically performed by state-of-the-art DL frameworks, such as TensorFlow, Keras, Caffe2, and other [74]. In Ex1, every layer has one phase. The CNN inference is performed in 5 computational steps. At every i-th computational step, $i \in [1,5]$, the single phase of layer l_i is executed. During its single

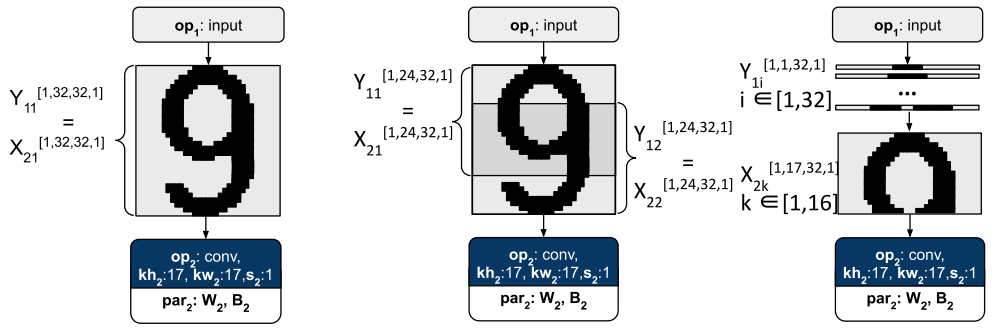

(a) *Ex1* **(b)** *Ex2* **(c)** *Ex3, Ex4*

Figure 4.2: *Input data processing by layer l_2*

phase, layer l_i processes its whole input data. Figure 4.2(a) shows how layer l_2 processes its input data in Ex1. Layer l_2 processes its whole input data X_2 as a single data part $X_{21} = X_2$. Data X_{21} is provided to layer l_2 by layer l_1 and stored in buffer B_1. To store data $X_{21}^{[1,32,32,1]}$ buffer B_1 occupies 1 * 32 * 32 *1 = 1024 bytes of memory.

Example Ex2, given in Row 4 of Table 4.1, shows how processing data by parts, combined with specific execution order of the phases, allows to reduce the CNN buffer sizes at the cost of decreasing the CNN throughput. In Ex2, CNN layer l_2 processes its input data X_2 in two overlapping parts, X_{21} and X_{22}, as shown in Figure 4.2(b). Data parts X_{21} and X_{22} are provided to layer l_2 by layer l_1 and stored in buffer B_1 during the CNN inference. The CNN inference is performed in 7 computational steps. At step 1, phase l_{11} is executed and data $Y_{11} = X_{21}$ is produced in B_1. At step 2, phase l_{21} is executed and data X_{21} is processed by layer l_2. After being processed, data X_{21} is not needed anymore and is removed from B_1. At step 3, phase l_{12} is executed and data $Y_{12} = X_{22}$ is produced in B_1. At step 4, phase l_{22} is executed and data X_{22} is processed by layer l_2. Steps 1 to 4 in Ex2 are functionally equivalent to steps 1 to 2 in Ex1. However, in Ex2 at every computational step, buffer B_1 has to store only a part of the input data ($X_{21}^{[1,24,32,1]}$ for steps 1 to 2 and $X_{22}^{[1,24,32,1]}$ for steps 3 to 4, respectively). Therefore, in Ex2, B_1 occupies 1* 24 * 32 * 1= 786 bytes of memory, instead of 1024 bytes, as in Ex1. Compared to Ex1, Ex2 reduces the total buffer sizes by 12% at the cost of only 0.3% throughput decrease due to the increased number of CNN computational steps in Ex2, compared to Ex1.

Example Ex3, given in Row 5 of Table 4.1, demonstrates one more way of executing layers l_1 and l_2 with phases, shown in Figure 4.2(c). In Ex3, layer l_1 has 32 phases and layer l_2 has 16 phases. The CNN inference is performed in 51 computational step. During the first 17 steps, phases l_{11}, l_{12}, ..., l_{117}, shortly written as $l_{1(1-17)}$, are executed. At every phase, layer l_1 produces

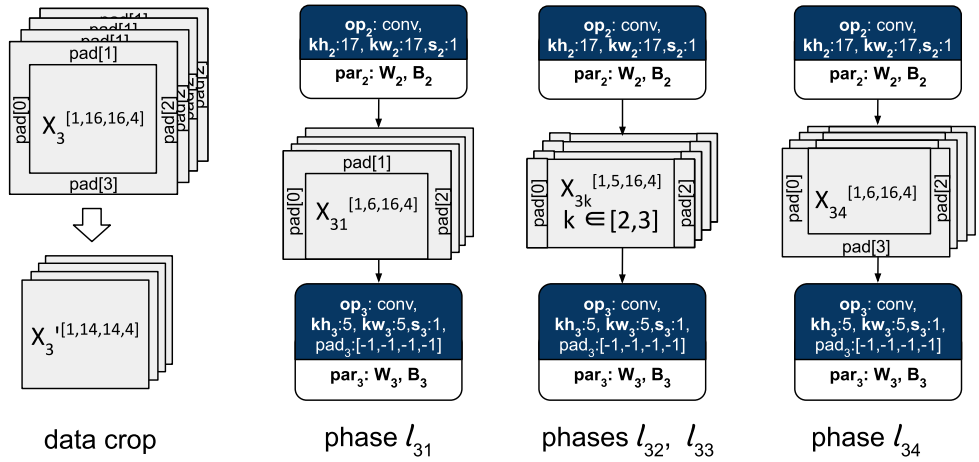

Figure 4.3: *Input data processing by layer l_3, Ex4*

data $Y_{1k}^{[1,1,32,1]} \subset X_{21}$ in buffer B_1, until sufficient data $X_{21}^{[1,17,32,1]}$ is accumulated. Then, at step 18, phase l_{21} is executed. To execute phase l_{22}, data $X_{22}^{[1,17,32,1]}$ should be accumulated in B_1. However, some of this data is already in B_1. As explained in Section 2.1, data between subsequent execution steps of layer l_2 is overlapping. If the overlapping part is stored in buffer B_1, only new (non-overlapping) data should be produced in B_1 to enable the execution of phase l_{22}. This new data can be produced by execution of one phase of layer l_1. Thus, phases 18-32 of layer l_1 and phases 2-16 of layer l_2 are executed in order $[l_{1(18-32)}, l_{2(2-16)}]$, meaning, that a phase of layer l_1 is followed by a phase of layer l_2, e.g., phase l_{118} is followed by phase l_{22}, and this pattern repeats, until all phases of layers l_1 and l_2 are executed. The maximum amount of data, stored between layers l_1 and l_2 per computational step corresponds to data part $X_{2k}^{[1,17,32,1]}$, accumulated in B_1. Thus, in Ex3, buffer B_1 occupies 1 * 17 * 32 * 1 = 544 bytes of memory. Compared to Ex1, Ex3 reduces the total buffer sizes by 23% at the cost of 7% throughput decrease.

Example Ex4, given in Row 6 of Table 4.1, demonstrates how several Convolutional layers in one CNN can be executed with phases, and how data padding is processed with phases. In Ex4, the CNN inference is executed in 54 computational steps. Layers l_1 and l_2 have 32 and 16 phases, respectively, as in Ex3. Additionally, layer l_3 has 4 phases, i.e., processes its input data in four parts. As explained in Section 2.1, layer l_3 has padding pad_3, which crops its input data. With data processing by parts, the data crop is also performed by parts, as shown in Figure 4.3. At phases l_{31} and l_{34}, layer l_3 accepts data $X_{3k}^{[1,6,16,4]}$ and crops it to data $X_{3k}^{\prime[1,5,14,4]}$. At phases l_{32} and l_{33}, it accepts data

$X_{3k}^{[1,5,16,4]}$ and crops it to data $X_{3k}^{\prime[1,5,14,4]}$. The maximum amount of data to be stored in B_2 is $X_{3k}^{[1,6,16,4]}$. Thus, buffer B_2 occupies 1 * 6 * 16 * 4 = 384 bytes of memory. Compared to Ex1, Ex4 reduces the total buffer sizes by 53% at the cost of 12.7% throughput decrease. As can be seen from Column 12 of Table 4.1, Ex4 is the most memory-efficient example among all presented examples.

The examples, provided in this section, demonstrate that there are many possible ways to execute the CNN inference with phases. Obtaining the most memory-efficient way is not trivial even for our small example CNN, shown in Figure 4.1, let alone for real-world state-of-the-art CNNs that are much larger and much more complex. Therefore, a systematic and automated methodology for finding the CNN inference execution with phases, which ensures minimum buffer sizes, is required. In the next section, we propose such a methodology.

4.5 Methodology

In this section, we present our three-step methodology for low-memory CNN inference at the Edge. Our methodology is shown in Figure 4.4. In Step 1 (Section 4.5.1), we automatically derive the number of phases for every CNN layer. The number of phases is computed such that at each phase, every CNN layer processes a minimum part of the layer input data and produces a minimum part of the layer output data. Thus, we ensure that every layer requires minimum amount of memory to store its input and output data at every phase. In Step 2 (Section 4.5.2), we model the CNN inference with phases, obtained at Step 1. We note that the CNN model, introduced in Section 2.1 and widely used to represent CNNs, does not have means for explicit specification of the CNN execution with phases, while the CSDF model, introduced in Section 2.5, has such means. Moreover, unlike the CNN model, the CSDF model is accepted as an input by many existing embedded systems

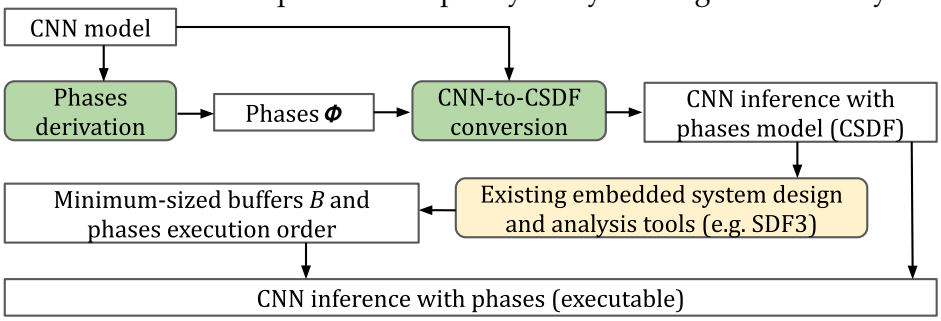

Figure 4.4: *Methodology for low-memory CNN inference*

design tools for automated performance/memory analysis, transformations and optimizations. Therefore, to enable for CNN execution with phases and utilization of existing embedded design tools, e.g., SDF3 [91], for the CNN analysis, in Step 2, we automatically convert a CNN model into a functionally equivalent CSDF model. In Step 3, we use the SDF3 tool to analyse the CNN and obtain a set of buffers B, used to store the intermediate computational results of the CNN, represented as the CSDF model at Step 2. Every buffer $B_k \in B$ is characterized with minimum size. Together with buffers B, the SDF3 tool obtains specific execution order of phases, which enables to correctly execute the CNN inference with buffers B. Thus, in our 3-step methodology, we use processing data by parts to ensure the CNN inference with minimum buffer sizes.

4.5.1 Phases derivation

In this section, we present our automated phases derivation algorithm - see Algorithm 3. Algorithm 3 accepts as an input a CNN, represented as the CNN model, explained in Section 2.1. As an output, Algorithm 3 provides a set of phases $\Phi = \{\Phi_1, \Phi_2, ..., \Phi_{|L|}\}$, where $\Phi_i \in \Phi$ is the number of phases, performed by layer l_i of the input CNN. For example, for the CNN shown in Figure 4.1, Algorithm 3 automatically derives a set of phases $\Phi = \{32, 16, 4, 1, 1\}$, which specifies that layers l_1, l_2, l_3, l_4, and l_5 of the CNN process data in $32, 16, 4, 1$, and 1 phases, respectively.

In Line 1, Algorithm 3 defines the set of phases Φ as an empty set. In Lines 2 to 8, Algorithm 3 computes the number of phases Φ_i for every layer l_i of the input CNN. Φ_i is computed such that at each phase, layer l_i accepts a part of the input data and produces the corresponding part of the output data. Each

Algorithm 3: Phases derivation

Input: $CNN(L, E)$
Result: Set of phases Φ

1 $\Phi \leftarrow \emptyset$;
2 **for** $l_i \in L$ **do**
3 **if** *size of* Θ_i = *size of* X_i **then**
4 $h^{out}_{min} = Y_i.h$;
5 **else**
6 $h^{out}_{min} = 1$;
7 $Y_{ik} \leftarrow$ part of Y_i of shape $[Y_i.batch, h^{out}_{min}, Y_i.w, Y_i.c]$;
8 $\Phi_i \leftarrow Y_i.h / Y_{ik}.h$;
9 $\Phi \leftarrow \Phi + \Phi_i$;
10 **return** Φ

part of input and output data of layer l_i is characterized with minimum height, determined by the attributes of layer l_i, shown in Table 2.1 and explained in Section 2.1. An example of such layer execution is shown in Figure 4.2(c), explained in Section 4.4, where layer l_2 performs $\Phi_2 = 16$ phases. At each phase $k \in [1, 16]$ layer l_2 accepts an input data part X_{2k} with minimum height of 17 pixels, and produces an output data part Y_{2k} with height of 1 pixel.

In Lines 3 to 6, Algorithm 3 computes the minimum height h_{min}^{out} of output data part Y_{ik}, produced by layer l_i at each phase. h_{min}^{out} is 1 pixel for every layer l_i, except of layers that process their input data at once (i.e., layers for which condition in Line 3 is met). In Line 7, Algorithm 3 defines output data part Y_{ik}, produced by layer l_i at each phase. Y_{ik} has the shape $[Y_i.batch, h_{min}^{out}, Y_i.w, Y_i.c]$, where $Y_i.batch$, $Y_i.w$, and $Y_i.c$ are the batch size, the width and the number of channels of output data Y_i, produced by layer l_i, and h_{min}^{out} is the minimum output data height, computed in Lines 3 to 6. In Line 8, Algorithm 3 computes the number of phases Φ_i performed by layer l_i as the number of output data parts with minimum height, produced by layer l_i. In Line 9, Algorithm 3 adds Φ_i to the set Φ. Finally, in Line 10, Algorithm 3 returns the set of phases Φ.

4.5.2 CNN-to-CSDF model conversion

The automated conversion of a CNN into a functionally equivalent CSDF model, utilized in our memory reduction methodology, is given in Algorithm 4. Algorithm 4 accepts as inputs a CNN, represented as the CNN model, explained in Section 2.1 and a set of phases Φ, automatically generated for the CNN by Algorithm 3 presented in Section 4.5.1. In Lines 1-16, explained in the *CSDF model topology generation* subsection below, Algorithm 4 generates the topology of the CSDF model $G(A, C)$. In Lines 17-36, explained in the *Production/consumption sequences derivation* subsection below, Algorithm 4 derives the production/consumption sequences for every channel in $G(A, C)$. Finally, in Line 37, Algorithm 4 returns $G(A, C)$, which is functionally equivalent to

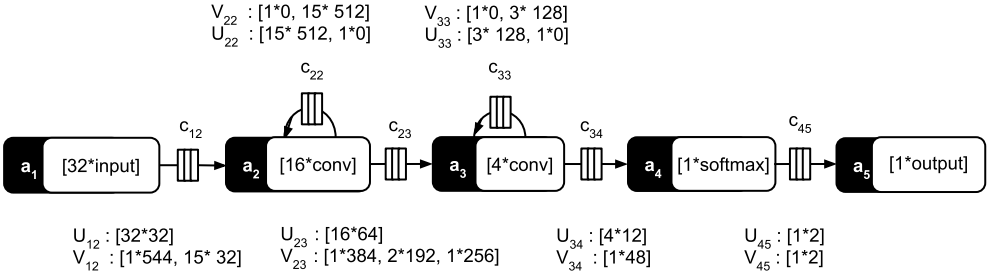

Figure 4.5: *CSDF model, derived from the CNN model shown in Figure 4.1*

the input $CNN(L, E)$ model. Figure 4.5 shows the CSDF model $G(A, C)$, automatically derived by Algorithm 4 from the CNN model $CNN(L, E)$ shown in Figure 4.1 and phases $\Phi = \{32, 16, 4, 1, 1\}$, derived for this CNN model by Algorithm 3. The examples, provided in this section for Algorithm 4, are referring to this CNN-to-CSDF conversion.

Algorithm 4: CNN-to-CSDF conversion

Input: $CNN(L, E), \Phi = \{\Phi_1, \Phi_2, ..., \Phi_{|L|}\}$
Result: $G(A, C)$

$A, C \leftarrow \emptyset$; $G(A, C) \leftarrow$ CSDF model (A, C) ;
foreach $l_i \in L$ **do**
  $F_i \leftarrow \emptyset$;
  $a_i \leftarrow$ actor (F_i);
  $A \leftarrow A + a_i$;
  $\{\Theta_i, op_i, s_i\} \leftarrow$ attributes of l_i (see Table 2.1);
  $P_i = \Phi_i$;
  for $p \in [1, P_i]$ **do**
    $f_i(p) = op_i$;
    $F_i = F_i + f_i(p)$;
  if $s_i < \Theta_i.h$ **then**
    $c_{ii} \leftarrow channel(a_i, a_i)$;
    $C \leftarrow C + c_{ii}$;
foreach $e_{ij} \in E$ **do**
  $c_{ij} \leftarrow channel(a_i, a_j)$;
  $C \leftarrow C + c_{ij}$;
foreach $c_{ij} \in C$ **do**
  $\{X_i, Y_i, kh_i, s_i, pad_i\} \leftarrow$ attributes of l_i (see Table 2.1);
  $\{X_j, Y_j, kh_j, s_j, pad_j\} \leftarrow$ attributes of l_j (see Table 2.1);
  if $i = j$ **then**
    for $p \in [1, P_i]$ **do**
      $u_{ij}(p) = \begin{cases} 0 & if \;\; p = P_i \\ X_i.batch * (\Theta_i.h - s_i) * X_i.w * X_i.ch & otherwise \end{cases}$
      $v_{ij}(p) = \begin{cases} 0 & if \;\; p = 1 \\ X_i.batch * (\Theta_i.h - s_i) * X_i.w * X_i.ch & otherwise \end{cases}$
  else
    for $p \in [1, P_i]$ **do**
      $u_{ij}(p) = Y_i.batch * 1 * Y_i.w * Y_i.ch$;
    $v_{ij}(1) = X_j.batch * (kh_j - pad_j[1]) * X_j.w * X_j.ch$;
    $hpad_j = \begin{cases} pad_j[1] + pad_j[3] & if \;\; P_j = 1 \\ pad_j[3] & otherwise \end{cases}$;
    if $\nexists c_{jj} \vee P_j = 1$ **then**
      for $p \in [2, P_j - 1]$ **do**
        $v_{ij}(p) = X_j.batch * kh_j * X_j.w * X_j.ch$;
      $v_{ij}(P_j) = X_j.batch * (kh_j - hpad_j) * X_j.w * X_j.ch$;
    else
      for $p \in [2, P_j - 1]$ **do**
        $v_{ij}(p) = X_j.batch * s_j * X_j.w * X_j.ch$;
      $v_{ij}(P_j) = X_j.batch * (s_j - hpad_j) * X_j.w * X_j.ch$;
return $G(A, C)$

CSDF model topology generation

The CSDF model topology generation is performed in Lines 1-16 of Algorithm 4. In Line 1, Algorithm 4 generates a new CSDF model $G(A, C)$ with an empty set of actors A and an empty set of communication channels C. In Lines 2-10 Algorithm 4 converts every layer l_i of the CNN model $CNN(L, E)$ into a functionally equivalent CSDF actor $a_i \in A$. Every actor $a_i \in A$ performs execution sequence $F_i = \{f_i(p)\}, p \in [1, P_i]$, where every function $f_i(p) \in F_i$ is specified as $f_i(p) = op_i$ (Lines 9-10 of Algorithm 4). On each phase $p \in [1, P_i]$, actor a_i applies operator op_i performed by layer l_i to the part of input data X_{ip} of the layer l_i and produces a part of output data Y_{ip}. Thus, actor a_i reproduces data processing by parts, performed by the layer l_i and explained in Section 4.4. The number of phases Φ_i of actor a_i representing layer l_i is specified in the input set of phases Φ. For example, actor a_3 performs execution sequence $F_3 = [P_3 * op_3] = [4 * conv]$, where $op_3 = conv$ is the operator, performed by layer l_3, 4 is the number of phases Φ_3, specified for layer l_3 in the input set of phases Φ.

In Lines 11-13 Algorithm 4 models overlapping data reuse, explained in Ex3 in Section 4.4. In Line 11, Algorithm 4 checks, if the data overlapping occurs in layer $l_i \in L$. If data overlapping occurs in layer l_i, in Lines 12-13 Algorithm 4 models data overlapping for corresponding actor a_i. Since the CSDF model does not allow internal state specification in actors, the data overlapping/reuse is modeled as self-loop FIFO channels c_{ii}, that store and reuse the overlapping data between subsequent firings of actor a_i. For example, the data overlapping occurs in layer l_3 ($s_3 = 3 < \Theta_3.h = 5$). Therefore, in Lines 12-13, Algorithm 4 creates self-loop channel c_{33}, which stores the overlapping/reuse data for actor a_3.

Finally, in Lines 14-16, Algorithm 4 converts every input CNN model edge $e_{ij} \in E$, representing a data dependency between layers $l_i \in L$ and $l_j \in L$, into communication FIFO channel $c_{ij} \in C$, representing data dependency between actors $a_i \in A$ and $a_j \in A$.

Production/consumption sequences derivation

The production sequence $U_{ij} = \{u_{ij}(p)\}$, $p \in [1, P_i]$ and the consumption sequence $V_{ij} = \{v_{ij}(p)\}$, $p \in [1, P_j]$ are derived for every channel $c_{ij} \in C$ of CSDF graph $G(A, C)$ in Lines 24 to 36 of Algorithm 4. For every data reuse channel $c_{ij} \in C, i = j$, storing the overlapping/reuse data between subsequent firings of actor a_i, the elements of the production/consumption sequences are computed in Lines 21 to 23 of Algorithm 4. Since at the last phase P_i of actor a_i there is no need to produce data to be reused, the last

element of the production sequence $u_{ij}(P_i)$ is set to 0 in Line 22 of Algorithm 4. Since at the first phase actor a_i has not yet produced data in the data reuse channel c_{ij}, the first element of the consumption sequence $v_{ij}(1)$ is set to 0 in Line 23 of Algorithm 4. For all other phases of actor a_i the elements of the production/consumption sequences are computed as the number of tokens in a tensor of shape $[X_i.batch, (\Theta_i - s_i), X_i.w, X_i.ch]$, reused between the subsequent firings of actor a_i. For example, data reuse channel c_{33} has production sequence $U_{33} : [3 * 128, 1 * 0]$ and consumption sequence $V_{33} : [1 * 0, 3 * 128]$.

For CSDF channels c_{ij}, that are not data reuse channels, i.e. $i \neq j$, the elements of the production/consumption sequences are computed in Lines 25 to 36 of Algorithm 4. The elements of the production sequence U_{ij} are computed as the number of elements in the output data part Y_{ip}, produced by actor a_i at phase p. For example, actor a_3 at its every phase $p \in [1, 4]$ produces data $Y_{3p}^{[1,1,4,3]}$, $p \in [1, 4]$, to channel c_{34}. Therefore, the elements of production rate of channel c_{34} are computed in Lines 25 to 26 of Algorithm 4 as $u_{34}(p) = 1 * 1 * 4 * 3 = 12$.

Every element of the consumption sequences $v_{ij}(p), p \in [1, P_j]$ is computed in Lines 27 to 36 of Algorithm 4 as the number of elements in data tensor, consumed by actor a_j from non-overlapping channel c_{ij} on the actors phase $p \in [1, P_j]$ in order to produce data Y_{jp}. The first element of the consumption sequences $v_{ij}(1)$ is computed in Line 27 of Algorithm 4. If no padding occurs at the first phase of actor a_j ($pad[1] = 0$ in Line 27 of Algorithm 4), actor a_j consumes from c_{ij} data X_{jp} with shape $[X_j.batch, X_j.ch, kh_j, X_j.w]$. If actor a_j crops data at the first phase ($pad_j[1] < 0$ in Line 27 of Algorithm 4), actor a_j consumes from c_{ij} data X_{jp} and data to be cropped. If actor a_j extends data at the first phase ($pad[1] > 0$ in Line 27 of Algorithm 4), actor a_j consumes from c_{ij} part of data X_{jp}, which is not provided by padding.

The computation of consumption sequence elements $v_{ij}(p), p \in [2, P_j]$ is divided in two different cases, determined by the presence of data overlapping in the channel sink actor a_j, corresponding to layer l_j. If data overlapping is not presented in actor a_j (Lines 29-32 of Algorithm 4), actor a_j consumes all input data from its non-overlapping input channel c_{ij}. If data overlapping/reuse is presented in actor a_j (Lines 34-36 of Algorithm 4), actor a_j consumes from channel c_{ij} only non-overlapping data. The overlapping/reuse data is consumed by actor a_j from its self-loop channel c_{jj}. In total, actor a_j consumes data X_{jp} at phases $p \in [2, P_j - 1]$ (Lines 30-31, 34-35 of Algorithm 4), and all the remaining data at phase $p = P_j$ (Lines 32, 36 of Algorithm 4). Consumption of all the remaining data from CSDF channels allows to empty the FIFO buffers

and ensure the CSDF model consistency [10].

For example, communication channel c_{23} has consumption sequence V_{23} : $[1 * 384, 2 * 192, 1 * 256]$. The first element of the consumption sequence is computed in Line 27 of Algorithm 4 as $v_{23}(1) = (5 - (-1)) * 16 * 4 = 384$, where $5 * 16 * 4 = 320$ elements are elements of input data tensor X_{31} of shape $[1, 5, 16, 4]$, used by actor a_3 to produce data Y_{31}, and $1 * 16 * 4 = 64$ elements are cropped by actor a_3 according to the padding pad_3. As data overlapping/reuse is presented for a_3 ($\exists c_{33}$), $v_{23}(p), p \in [2, 4]$ are computed in Lines 34-36 of Algorithm 4. At phases $p \in [2, 3]$ actor a_3 consumes non-overlapping data $3 * 16 * 4 = 192$ from channel c_{23}, i.e., $v_{23}(p) = 192, p \in [2, 3]$. At the last phase actor a_3 consumes the remaining data $(3 - (-1)) * 16 * 4 = 256$ from channel c_{23}, i.e. $v_{23}(4) = 256$.

4.6 Experimental Results

In this section, we evaluate our memory reduction methodology in terms of achieved memory footprint reduction as well as we show the cost of this memory footprint reduction in terms of decreased CNN inference throughput. To this end, we take real-world CNNs from the ONNX models Zoo [7] and obtain their memory footprint and inference throughput, when the memory footprint of the CNNs is reduced using: 1) the most relevant CNN buffers reuse methodology, briefly introduced in Section 4.3, and employed by the TensorRT framework for efficient CNN execution at the Edge [72]; 2) our memory reduction methodology, presented in Section 4.5. The results of the experiment are given in Table 4.2.

We perform our experiment in two steps. In Step 1, for every CNN from the ONNX models Zoo, we derive: 1) a TensorRT C++ executable application, which represents the CNN inference with the TensorRT buffers reuse

Table 4.2: *Evaluation of our memory reduction methodology*

CNN	Memory footprint (MB)		Memory reduction (%)	Throughput (fps)		Throughput reduction (%)
	TensorRT	ours		TensorRT	ours	
resnet18	51.6	49	5	137	121	12
googlenet	38.7	31	19.8	118	103	13
tiny yolo v2	77.3	64.3	16.8	131	105	20
inception v1	38.3	31	19	122	106	13
VGG 19	594	577	2.8	15	14.7	2
densenet121	43	40	7.5	62	49	21
squeezenet	10.4	6.4	38	342	262	23

methodology. This application is automatically generated by the TensorRT DL framework from the input CNN description in .onnx format; 2) a C++ CNN inference with phases application, which implements the CNN inference with phases, derived from the same input CNN by our methodology presented in Section 4.5. To implement this application, we use the TensorRT DL framework as well as a custom code generation component, which offers support of the CNN inference with phases (CSDF) model, unsupported by the TensorRT DL framework. The TensorRT DL framework is used to define CNN operators, while our custom code is used to define the CSDF model.

In Step 2, we execute the applications, obtained in Step 1. We measure and compare the memory footprint as well as the throughput of the CNNs, when the memory footprint of the CNNs is reduced using: 1) the TensorRT buffers reuse methodology; 2) our memory reduction methodology. Columns 2 and 3 in Table 4.2 show the memory footprint (in MegaBytes) of every CNN, i.e., the total amount of memory required to store the CNN parameters (weights and biases) together with the CNN intermediate computational results. Column 4 in Table 4.2 shows the memory reduction (in %), achieved by our methodology in comparison with the TensorRT DL framework. It shows that our methodology achieves 2.8% to 38% memory reduction, compared to the TensorRT buffers reuse methodology. The difference in memory reduction can be explained using the CNN characteristics shown in Table 4.3. First of all, as explained in Section 4.5, our methodology only reduces the amount of memory required to store the intermediate computational results of a CNN. Therefore, our methodology is most efficient for CNNs for which the intermediate computational results (stored in the CNN buffers as explained in Section 2.2) constitute the largest part of the total CNN memory requirement. Columns 2 to 4 in Table 4.3 show the amount of memory (in MegaBytes) required to store intermediate computational results (see Columns 2 and 3) and parameters (see Column 4) of the CNNs from the ONNX models Zoo. For example, the

Table 4.3: *CNN characteristics affecting CNN memory reduction and throughput decrease*

CNN	Buffer sizes (MB)		parameters (MB)	Total phases	
	TensorRT	ours		TensorRT	ours
resnet18	4.8	2.2	46.8	68	1962
googlenet	10.7	3	28	143	2630
tiny yolo v2	14.2	0.8	63.5	33	3796
inception v1	10.3	3	28	143	2494
VGG 19	19.3	2.3	574.7	46	2354
densenet121	10.9	7.9	32.1	428	8935
squeezenet	5.1	1.4	5	66	1870

squeezenet CNN (see Row 9 in Table 4.3) requires 1.4 to 5.1 MegaBytes of memory to store its intermediate computational results and and 5 MegaBytes of memory to store its parameters. Analogously, the VGG 19 CNN (see Row 7 in Table 4.3) requires 2.3 to 19.3 MegaBytes of memory to store its intermediate computational results and 574.5 MegaBytes of memory to store its parameters. In other words, the squeezenet CNN requires similar amount of memory to store its intermediate computational results and its parameters, while the VGG 19 CNN requires much more memory to store its parameters than to store its intermediate computational results. Consequently, our methodology achieves a significant, 38%, memory reduction for the squeezenet CNN and small, 2.8%, memory reduction for the VGG 19 CNN (see Row 7 and Row 9, Column 4 in Table 4.2). Secondly, as explained in Section 4.3, unlike the TensorRT buffers reuse methodology, our methodology reuses data within CNN layers. As shown in Section 4.4, the more phases are performed by layers of a CNN, the more memory is reused within the CNN layers and the more memory reduction can our methodology achieve. Thus, the number of phases performed by the CNN layers affects the memory reduction, achieved by our methodology. The number of phases performed by the CNN layers, when the CNNs are executed with the TensoRT buffers reduction methodology and with our methodology, is shown in Columns 5 and 6 in Table 4.3, respectively. When a CNN is executed with the TensoRT buffers reduction methodology, every layer of the CNN performs one phase. Therefore, the total number of phases performed by the layers of a CNN corresponds to the number of layers in the CNN. When a CNN is executed with our methodology, the total number of phases performed by the CNN layers is computed as $\sum_{\Phi_i \in \Phi} \Phi_i$, where Φ is a set of phases, derived for the CNN using Algorithm 3 introduced in Section 4.5.1. For example, Row 5, Columns 5 and 6 in Table 4.3 shows that the tiny yolo v2 CNN performs 33 phases when is executed with the TensoRT buffers reduction methodology and 3796 phases when executed with our methodology. We believe that the high, 16.8%, memory reduction, achieved by our methodology for the tiny yolo v2 CNN (see Column 4, Row 5 in Table 4.2) is due to the large amount of memory reuse within the CNN layers that our methodology introduced into the tiny yolo v2 CNN by increasing the total number of CNN phases $3796/33 \approx 115$ times.

Columns 5 and 6 in Table 4.2 show the throughput (in frames per second), demonstrated by the CNNs executed with the TensorRT buffers reuse methodology and our methodology, respectively. Column 7 shows the throughput decrease (in %), introduced into the CNNs inference by our methodology. It shows that our methodology decreases the CNN throughput by 2% to 23%,

depending on the CNN. As mentioned in Section 4.4, the throughput decrease, possibly introduced in a CNN by our proposed methodology, depends on the amount of phases performed by the CNN layers. The more phases are performed by the CNN layers, the larger is the possible throughput decrease. For example, our methodology introduces more throughput decrease into the tiny yolo v2 CNN than into the resnet18 CNN (see Row 3 and Row 5 in Table 4.2), because it introduces more phases in the tiny yolo v2 CNN than in the resnet18 CNN (see Row 3 and Row 5, Column 6 in Table 4.3). However, being a relative value, the amount of throughput decrease also depends on the overall CNN throughput. For example, the throughput reduction is larger for the squeezenet CNN than for the VGG 19 CNN (see Row 7 and Row 9 in Table 4.2), because the squeezenet CNN has much higher throughput than the VGG 19 CNN, and thus is more sensitive to the throughput decrease, introduced by our methodology.

4.7 Conclusion

We propose a novel CNN memory footprint reduction methodology. Our proposed methodology is based on the ability of CNN operators to process data by parts. By splitting input and output data of CNN layers into parts, and efficiently reusing the platform memory among these parts, our methodology allows to reduce the CNN memory footprint at the cost of decreasing the CNN throughput. The key feature of our methodology is the exploitation of CNNs ability to process data by parts for the CNN memory footprint reduction. The evaluation results show that, compared to the memory reduction, achieved by the most relevant CNN buffers reuse methodology, employed by the TensorRT DL framework for efficient CNN execution at the Edge, our memory reduction methodology allows to reduce the CNN memory footprint by 2.8% to 38% at the cost of 2% to 23% decrease of the CNN throughput.